

Background



Computation and Results



STRIPPED DOWN CLUSTER GALAXIES WITH GRAVITATIONAL LENSING

PART III PRESENTATION

JOE WINTERBURN

INSTITUTE OF ASTRONOMY

16TH MARCH 2021

Background

-
-
-
-
-
-

Computation and Results

-
-
-

OUTLINE

1 Background

- Motivations
- Horizon AGN
- Gravitational Lensing
- Weak Lensing
- Strong Lensing
- Limitations

2 Computation and Results

- Weak Lensing: Convergence and Shear
- Radial Profiles
- Strong Lensing: Caustics



MOTIVATIONS

- Lensing directly measures fractional energy density of matter.
- Lensing statistics can be used to probe properties of galaxy populations.
- The effects of tidal stripping in satellite vs central populations can be explored.
- Lensing doesn't rely on assumptions about dynamical environment or dark matter distribution.
- Computing lensing statistics in hydrodynamical simulations and comparing to observation allows constraints to be put on models.

STRIPPED DOWN CLUSTER GALAXIES WITH GRAVITATIONAL LENSING

- └ Background
- └ Motivations
- └ MOTIVATIONS

MOTIVATIONS

- Lensing directly measures fractional energy density of matter.
- Lensing statistics can be used to probe properties of galaxy populations.
- The effects of tidal stripping in satellite vs central populations can be explored.
- Lensing doesn't rely on assumptions about dynamical environment or dark matter distribution.
- Computing lensing statistics in hydrodynamical simulations and comparing to observation allows constraints to be put on models.

Lensing is a useful probe for Ω_m in the universe.

Quantities (convergence, shear, magnification) and statistics (correlation functions, galaxy-galaxy signal) can be computed for galaxy populations. Correlation functions can show differences between these two galaxy populations, and these can be put into context of the galactic halo model.

Makes it a very useful probe for imaging surveys.

Some research has been done on this recently, more on that to come.

Background



Motivations

Computation and Results



- (Bahé 2021) recently explored the claim that cluster subhaloes are more abundant than Λ CDM predictions.
- (Meneghetti et al. 2020) highlighted this issue and proposed that either there are systematic issues with simulations or incorrect assumptions about dark matter.
- (Bahé 2021) concludes that there is no tension with Λ CDM models, but the observed abundances can provide constraints on baryonic physics in simulations.
- The take-away is that one needs to be careful about limiting resolution on small scales in cosmological simulations.

Background



Horizon AGN

Computation and Results



HORIZON AGN

The data made available to me is from the Horizon AGN simulation:

- Cosmological hydrodynamical simulation performed with RAMSES.
- 1024^3 dark matter particles.
- Mass resolution of $8 \times 10^7 h^{-1} M_{\odot}$.
- Lensing quantities (deflection) generated by multiple lens-plane raytracing through the lightcone.
- Field of view: 1 deg^2 up to $z \approx 7$, 2.25 deg^2 up to $z \approx 1$.

STRIPPED DOWN CLUSTER GALAXIES WITH GRAVITATIONAL LENSING

- └ Background
 - └ Horizon AGN
 - └ HORIZON AGN

HORIZON AGN

The data made available to me is from the Horizon AGN simulation:

- Cosmological hydrodynamical simulation performed with RAMSES.
- 1024^3 dark matter particles.
- Mass resolution of $8 \times 10^7 h^{-1} M_{\odot}$.
- Lensing quantities (deflection) generated by multiple lens-plane raytracing through the lightcones.
- Field of view: 1 deg^2 up to $z \approx 7$, 2.25 deg^2 up to $z \approx 1$.

I believe the raytracing was performed at each simulation time step during the dynamical simulation.

The deep lightcone deflection map is a product of considering 500 transverse lens planes with varying comoving thickness.

Background



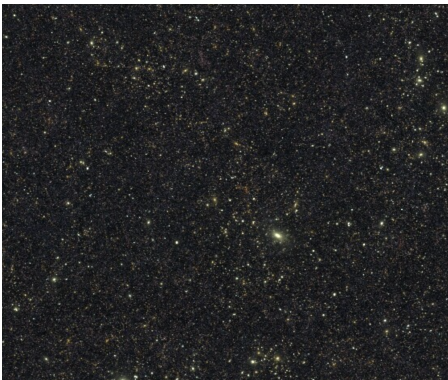
Horizon AGN

Computation and Results



Horizon AGN also provides predictions for flux, based on stars:

- Star properties: mass, age, metallicity → spectrum;
- These are combined to give a flux prediction. An image of the simulated flux is shown.



Background



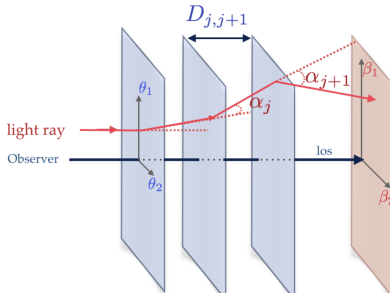
Horizon AGN

Computation and Results



The deflection field is computed from the same gravitational acceleration field used to evolve Eulerian quantities in the hydrodynamical simulation. These deflection maps were given to me as the starting point for my work.

- This is performed recursively for each lens plane.
- Goes beyond the Born approximation.

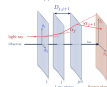


STRIPPED DOWN CLUSTER GALAXIES WITH GRAVITATIONAL LENSING

- └ Background
 - └ Horizon AGN

The deflection field is computed from the same gravitational acceleration field used to evolve Eulerian quantities in the hydrodynamical simulation. These deflection maps were given to me as the starting point for my work.

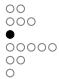
- This is performed recursively for each lens plane.
- Goes beyond the Born approximation.



Limitations arise if cells on the boundary of adjacent slabs are updated inbetween the simulation timesteps, but this is rare.

Born approximation: integrate along straight-line line of sight.

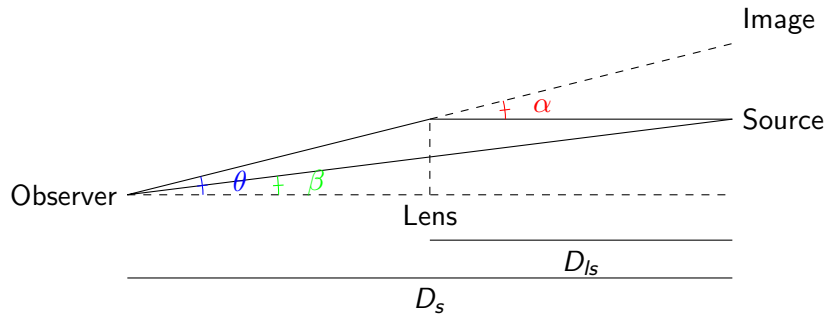
Background



Gravitational Lensing

GRAVITATIONAL LENSING

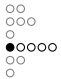
Einstein's General Relativity predicts the gravitational deflection of photons by mass distributions, famously confirmed experimentally by Eddington in 1919.



Computation and Results



Background



Weak Lensing

Computation and Results



The thin lens approximation gives the following relationship between the unobservable true source position $\vec{\beta}$ and the observed image position $\vec{\theta}$:

$$\vec{\beta} = \vec{\theta} - \frac{D_{ls}}{D_s} \vec{\alpha}(\vec{\theta}). \quad (1)$$

STRIPPED DOWN CLUSTER GALAXIES WITH GRAVITATIONAL LENSING

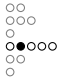
- └ Background
 - └ Weak Lensing

The thin lens approximation gives the following relationship between the unobservable true source position $\vec{\beta}$ and the observed image position $\vec{\theta}$:

$$\vec{\beta} = \vec{\theta} - \frac{D_b}{D_h} \vec{\alpha}(\vec{\theta}). \quad (1)$$

This mapping is the basis from which most quantities are derivable. The deflection angle α is exactly that which is produced by the raytracing. This mapping is also useful for cross referencing lenses to sources in lensing events, as the image positions can be projected into the source plane.

Background



Weak Lensing

Computation and Results

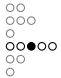


A Taylor expansion of the lens equation 1 gives the Jacobian of the $\vec{\theta} \rightarrow \vec{\beta}$ mapping, defining the magnification tensor

$$a_{ij}(\vec{\theta}) = \frac{\partial \vec{\beta}}{\partial \vec{\theta}} = \delta_{ij} - \phi_{,ij} \equiv \begin{pmatrix} 1 - \kappa - \gamma_1 & -\gamma_2 \\ -\gamma_2 & 1 - \kappa + \gamma_1 \end{pmatrix} \quad (2)$$

with ϕ the lensing potential, related to the convergence κ by $\Delta\phi = \nabla \cdot \vec{\alpha} \equiv 2\kappa$, and $\gamma_{1/2}$ the components of the spin-2 shear.

Background



Weak Lensing

Computation and Results



The lensing observables can be calculated by

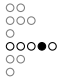
$$\kappa = \frac{1}{2} (\alpha_{1,1} + \alpha_{2,2}) \quad (3)$$

$$\gamma_1 = \frac{1}{2} (\alpha_{1,1} - \alpha_{2,2}) \quad (4)$$

$$\gamma_2 = \alpha_{1,2} = \alpha_{2,1} \quad (5)$$

which can be computed numerically using finite differences.

Background



Weak Lensing

Computation and Results



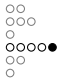
The convergence is the projected surface mass density in the lens plane expressed in units of the critical density:

$$\Sigma_{\text{crit}} \kappa(\theta) = \Sigma(\theta) = \int \rho(\theta, z) dz. \quad (6)$$

where the critical density is defined by

$$\Sigma_{\text{crit}} = \frac{c^2}{4\pi G} \frac{D_s}{D_l D_{ls}}. \quad (7)$$

Background



Weak Lensing

Computation and Results



From (Gouin et al. 2019), the tangential shear, convergence and mean convergence enclosed inside a radius R around a lensing galaxy/halo are related by

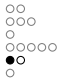
$$\bar{\kappa}(< R) = \frac{2}{R^2} \int_0^R \kappa(R') R' dR' = \kappa(R) + \gamma(R). \quad (8)$$

Using the definition of Σ_{crit} in equation 7, the excess density $\Delta\Sigma$ can be defined as

$$\Delta\Sigma(R) = \frac{M(< R)}{\pi R^2} - \Sigma(R) = \Sigma_{\text{crit}} \gamma(R). \quad (9)$$

So correlation functions can be computed around a selection of lensing galaxies and the statistics can be related to Σ and $\Delta\Sigma$.

Background

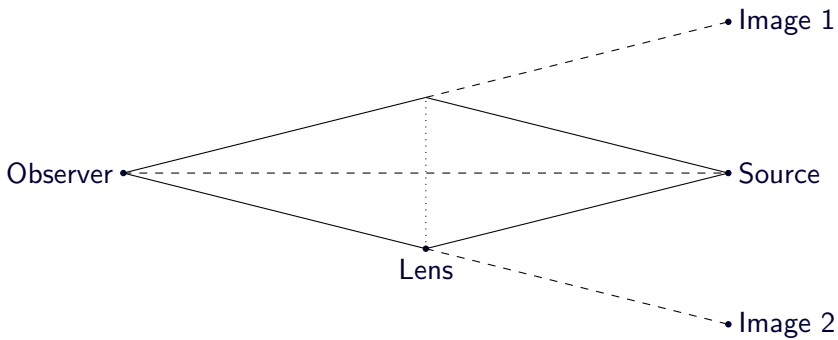


Strong Lensing

Computation and Results



In the strong lensing regime, multiple images can be produced from a single source:



This occurs when light rays pass through a region in which the lensing potential is sufficiently strong.

Background



Strong Lensing

Computation and Results



- The mapping $\beta \rightarrow \theta$ is no longer bijective.
- Regions in the source plane that correspond to multiple images are caustic regions.
- The area of such regions is related to the optical depth for strong lensing τ .
- Galaxy catalogs can be projected into the source plane and matched with caustics, allowing cross sections to be related to galactic properties.

Background



Limitations

LIMITATIONS

Computation and Results



- Larger source redshifts mean more potential for noise as the deflection is found by integrating along the line of sight, so intermediate matter will feature in the calculation.
- Exploring small scales is limited by the resolution of the simulation as mentioned before, and the resolution of the deflection maps.
- Isolating galaxies at a range of redshifts means lensing efficiency will vary depending on the distances involved.

Background



Weak Lensing: Convergence and Shear

Computation and Results



CONVERGENCE AND SHEAR MAPS

Convergence and tangential shear maps were computed from the Jacobian of the deflection fields for source redshifts

$z_s = 0.39, 1.5, 4.89$ for the narrow 1 deg^2 field of view, and

$z_s = 0.97$ for the wider 2.25 deg^2 field, using finite differences.

The resulting maps for the largest redshift in the narrow field, and the wide field are shown:

Background

○○
○○○
○
○○○○○
○○○

Computation and Results

●○○○○
○○○○○○○○○○
○○○○

Weak Lensing: Convergence and Shear

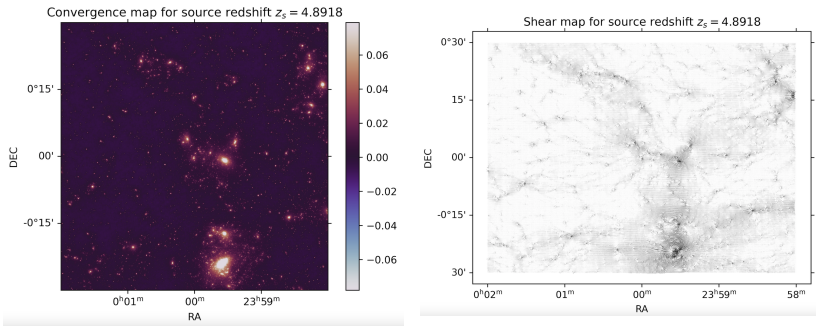


Figure: Convergence and tangential shear for $z_s = 4.89$

Background



Computation and Results



Weak Lensing: Convergence and Shear

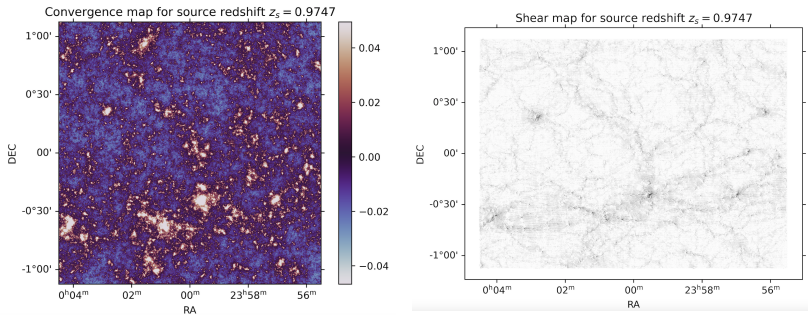


Figure: Convergence and tangential shear for $z_s = 0.97$

Background

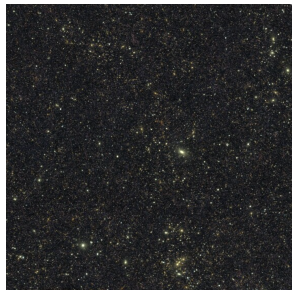
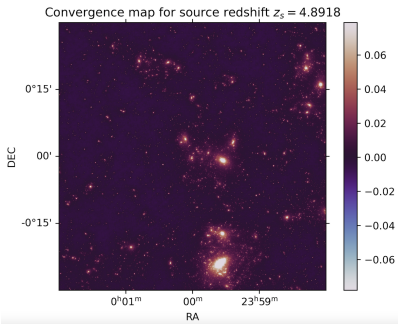


Computation and Results



Weak Lensing: Convergence and Shear

As the convergence corresponds to the lensing mass distribution, it is instructive to compare the convergence profiles with the simulated light distribution from the simulation:



A clear correspondence with the convergence map and light distribution can be seen.

Background

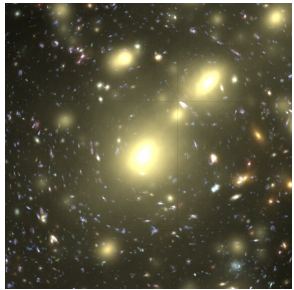
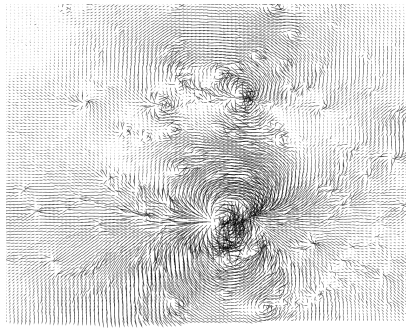
○○
○○○
○
○○○○○
○○
○

Weak Lensing: Convergence and Shear

Computation and Results

○○○○●○
○○○○○○○○○○
○○○○

Zooming into the main cluster, one can compare the tangential shear to the observed tangential alignment of background sources:





Weak Lensing: Convergence and Shear



- Catalogs of galaxies are provided for the Horizon AGN simulation.
- The radial profile of κ and γ_t were calculated for each galaxy.
- Radial bins from $R = 0.02$ Mpc to $R = 5$ Mpc were considered.
- Galaxies near the edge of the field of view were excluded as the radial information would be incomplete.
- This loss is acceptable as the deflection field is not always well defined near the edge of the field of view due to artefacts arising from the method of calculation within the raytracing step.

Background

○○
○○○
○
○○○○○
○○
○

Radial Profiles

Computation and Results

○○○○○○○
●○○○○○○○○○
○○○○

Lensing galaxies in small redshift slices are stacked, comparing satellite to central galaxies, and distinguishing stellar mass bins. Some resulting plots are shown below:

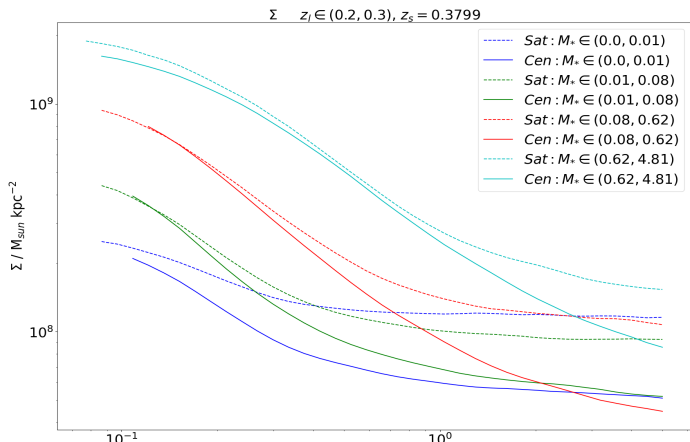
Background

○○
○○○
○
○○○○○
○○
○

Computation and Results

○○○○○○○
○●○○○○○○○○
○○○○

Radial Profiles



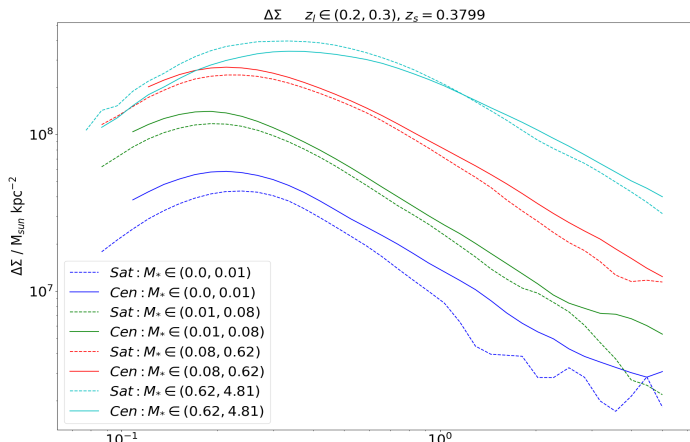
Background

○○
○○○
○
○○○○○
○○
○

Computation and Results

○○○○○○○
○○●○○○○○○○
○○○○○

Radial Profiles



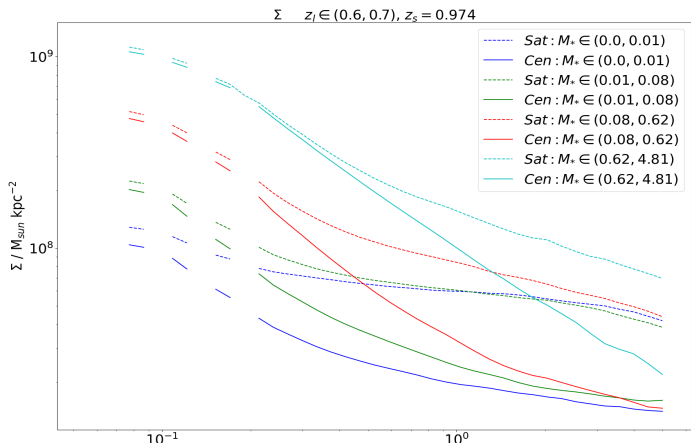
Background

○○
○○○
○
○○○○○
○○○
○

Computation and Results

○○○○○○○
○○○●○○○○○○
○○○○

Radial Profiles



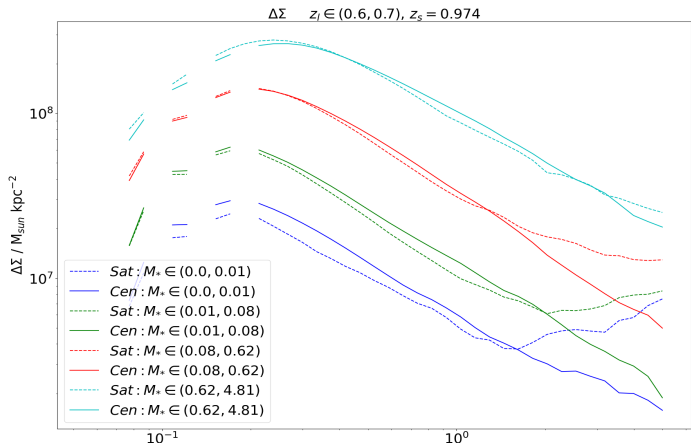
Background

○○
○○○
○
○○○○○
○○○
○

Computation and Results

○○○○○○○
○○○○●○○○○○
○○○○○

Radial Profiles



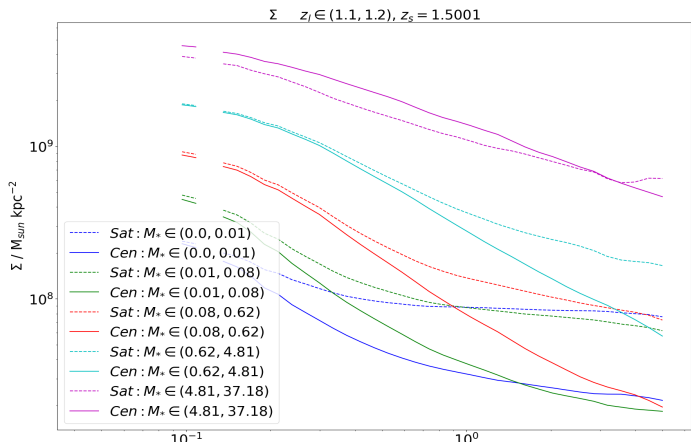
Background

○○
○○○
○
○○○○○
○○
○

Computation and Results

○○○○○○
○○○○○●○○○○
○○○○

Radial Profiles



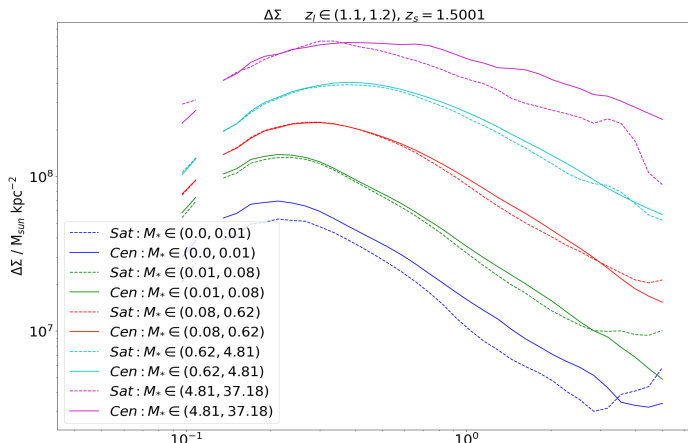
Background

○○
○○○
○
○○○○○
○○
○

Computation and Results

○○○○○○
○○○○○●○○
○○○○

Radial Profiles



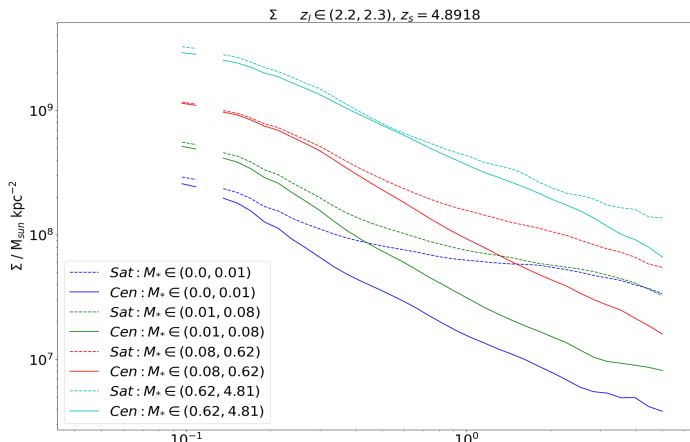
Background

○○
○○○
○
○○○○○
○○
○

Computation and Results

○○○○○○
○○○○○○○●○○
○○○○

Radial Profiles



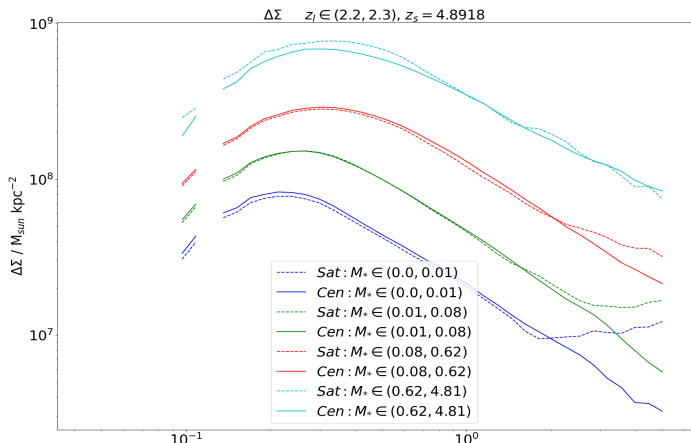
Background

○○
○○○
○
○○○○○
○○○
○

Computation and Results

○○○○○○○
○○○○○○○○●○
○○○○

Radial Profiles



Background



Radial Profiles

Computation and Results



The results are as expected:

- An increase in stellar mass always corresponds to an increase in overall Σ .
- Satellites have a flatter Σ and $\Delta\Sigma$ profile at large radii.
- The flatter profile and fluctuations in $\Delta\Sigma$ can be put into context of the galactic halo model:
 - The $\Delta\Sigma$ profiles peak around the 1-halo term ($\Delta\Sigma_{1h}$) corresponding to the main halo of the host galaxy.
 - Σ profiles are much flatter in the tail as compared to centrals; satellites are expected to reside in the vicinity of a larger halo, so this corresponds to the 2-halo term (Σ_{2h}).

STRIPPED DOWN CLUSTER GALAXIES WITH GRAVITATIONAL LENSING

- └ Computation and Results
 - └ Radial Profiles

- The results are as expected:
- u An increase in stellar mass always corresponds to an increase in overall Σ .
 - u Satellites have a flatter Σ and $\Delta\Sigma$ profile at large radii.
 - u The flatter profile and fluctuations in $\Delta\Sigma$ can be put into context of the galactic halo model:
 - o The $\Delta\Sigma$ profiles are dominated by 1-halo term ($\Delta\Sigma_{\text{1h}}$) compared to the main term of the host galaxy.
 - o Σ profiles are much flatter in the tail as compared to central; satellites are expected to reside in the vicinity of a larger halo, so this corresponds to the 2-halo term (Σ_{2h}).

The gaps for smaller scales are due to the limiting resolution of the convergence/shear maps. This becomes more prominent at larger lens plane redshifts.

Background



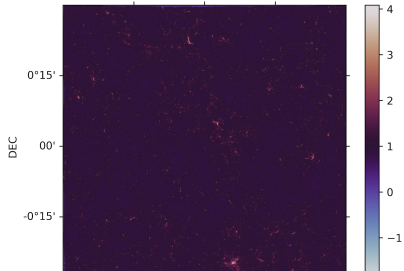
Strong Lensing: Caustics

Computation and Results



CAUSTICS

Caustic maps for the range of source redshifts were computed by exploring the mapping from image to source plane $\theta \rightarrow \beta$. Areas in the source plane onto which multiple image positions are mapped were computed, generating caustic maps of the source plane. An example of such a map is given below:



Background

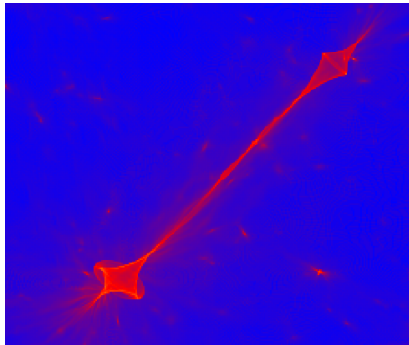
○○
○○○
○
○○○○
○○
○

Computation and Results

○○○○○
○○○○○○○○○
○●○○

Strong Lensing: Caustics

Below is a close up of the caustic region corresponding to the largest cluster in the field. Note the astroidal shape, with cusp singularities expected with lensing caustics.



Background



Strong Lensing: Caustics

Computation and Results



- Area of caustics → optical depth/strong lensing cross section.
- SExtractor has been used to build catalogs of individual caustoc regions above a magnification threshold ($\mu > 10$).
- Galaxy positions in lens planes are projected into the source plane using the lens equation, and are linked to particular caustic regions.
- The most likely caustic region for each lensing galaxy is found using a nearest neighbours algorithm.

Background

○○
○○○
○
○○○○
○○
○

Strong Lensing: Caustics

Computation and Results

○○○○○
○○○○○○○○○○
○○○●

- The plan is to use this information to relate galactic properties (M_* , halo environment) to strong lensing cross section. I am yet to carry out this analysis.
- An obvious issue that will arise is overcounting of caustic areas due to clustering - this will show up easily in the results and can hopefully be highlighted.